

A Surface-Tension Driven Micropump for Low-Voltage and Low-Power Operations

Kwang-Seok Yun, Il-Joo Cho, Jong-Uk Bu, Chang-Jin (CJ) Kim, and Euisik Yoon

Abstract—In this paper, we first report a micropump actuated by surface tension based on continuous electrowetting (CEW). We have used the surface-tension-induced motion of a mercury drop in a microchannel filled with an electrolyte as actuation energy for the micropump. This allows low voltage operation as well as low-power consumption. The micropump is composed of a stack of three wafers bonded together. The microchannel is formed on a glass wafer using SU-8 and is filled with electrolyte where the mercury drop is inserted. The movement of the mercury pushes or drags the electrolyte, resulting in the deflection of a membrane that is formed on the second silicon wafer. Another silicon wafer, which has passive check valves and holes, is stacked on the membrane wafer, forming inlet and outlet chambers. Finally, these two chambers are connected through a silicone tube forming the complete micropump. The performance of the fabricated micropump has been tested for various operation voltages and frequencies. We have demonstrated actual liquid pumping up to 70 $\mu\text{L}/\text{min}$ with a driving voltage of 2.3 V and a power consumption of 170 μW . The maximum pump pressure is about 800 Pa at the applied voltage of 2.3 V with an operation frequency of 25 Hz. [713]

Index Terms—Continuous electrowetting, liquid metal, low power, low voltage, microfluidics, micropump, surface tension.

I. INTRODUCTION

THERE is strong demand for miniaturized flow control devices, including micropumps, microvalves, and micromixers in the fields of miniaturized chemical analysis systems such as micro total analysis systems (μTAS) or lab-on-a-chip, as well as embedded medical devices, micro-dosing systems, and miniaturized production systems. Micromachining and microelectromechanical systems (MEMS) technology have increased the performance and functionality of such microfluidic devices with cost effective miniaturization and has made it possible to integrate them with microsensors and control circuitry, which has opened the new application fields mentioned above.

The micropump is a key component that exerts a force on a liquid to sample blood or water, dose a drug, and allow liquid to flow. Though some micropumps are nonmechanical types utilizing electrohydrodynamic, electroosmotic, ultrasonic or

thermocapillary forces, most micropumps are mechanical types composed of mechanically moving membranes. This is because mechanical micropumps can be used for wide applications without any restrictions in pumping liquid [1]. Previously, a number of mechanical micropumps have been developed using various mechanisms, including piezoelectric [2]–[4], electrostatic [5], [6], thermopneumatic [7]–[9], electromagnetic [10], bimetallic [11] and shape memory alloy (SMA) actuations [12]. However, most of them require either high operation voltages (piezoelectric and electrostatic actuations) or high operation powers (thermopneumatic, electromagnetic and SMA actuations). These devices are difficult to apply in certain application fields such as portable embedded medical devices, remote environmental monitoring systems, handheld chemical analyzers, etc., where both low voltage and low power operation are crucial factors.

At microscale, surface tension is a relatively large force compared to other forces such as gravity or structural stiffness, and has been a serious hindrance to the successful fabrication and operation of microdevices. Electrocapillary and electrowetting, including continuous electrowetting (CEW), are interesting phenomena which show active use of strong surface tension at microscale. Beni *et al.* demonstrated the surface-tension-driven motion of a mercury drop in a glass capillary and applied this principle to an optical switch [13], [14]. A micropump using the electrocapillarity of mercury was first theorized by Matsumoto and Colgate [15], and was recently realized by Ni *et al.*, who fabricated the pump using traditional manufacturing methods [16]. In recent years, Lee *et al.* reported MEMS devices, which employ the CEW phenomenon for generating linear and circular motions of a mercury drop with a small driving voltage of about 3 V and low power consumption (10–100 μW) [17]. We have applied this actuation mechanism for a micropump in which the pumping membranes are deflected according to the pressure induced by the mercury movement in a microchannel. In this paper, we report the working principle of the proposed micropump followed by its fabrication process and experimental results.

II. PRINCIPLE OF ACTUATION MECHANISM

Electrowetting is an electrically-induced change of a material's wettability. Fig. 1 shows a schematic illustration of continuous electrowetting. Initially, without bias voltage, a liquid metal (typically mercury; gallium was tested for CEW in previous report [13] as well as low-melting-temperature alloys [18], but not for the devices in this work). in a capillary filled with an electrolyte has a uniformly distributed charge density along the x -direction. If a voltage is applied between

Manuscript received June 27, 2001; revised March 23, 2002. This work was supported in part by the Korea Science and Engineering Foundation through the MICROS center at KAIST and the National Research Laboratory program from the Ministry of Science and Technology of Korea. Subject Editor K. D. Wise.

K.-S. Yun, I.-J. Cho, and E. Yoon are with the Department of Electrical Engineering and Computer Science, Korea Advanced Institute of Science and Technology (KAIST), Daejeon 305-701, Korea (e-mail: ksyun@iml.kaist.ac.kr).

J.-U. Bu is with LG Electronics Institute of Technology (LG Elite), Seoul 137-724, Korea.

C.-J. Kim is with the Mechanical and Aerospace Engineering Department, University of California, Los Angeles, CA 90095-1597 USA.

Digital Object Identifier 10.1109/JMEMS.2002.803286.

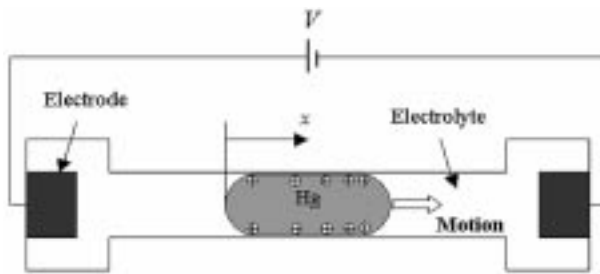


Fig. 1. Schematic illustration of continuous electrowetting.

two electrodes, the electric potential difference between the mercury and electrolyte varies along the x -direction and this induces charge redistribution. The more highly charged the interface becomes, the more the charges repel each other, thereby decreasing the cohesive forces and lowering the surface tension. Therefore, the surface tension on the right-hand side of the mercury is less than that on the left-hand side. This gradient in surface tension induces motion of the mercury to the right, as shown in Fig. 1.

III. DESIGN AND WORKING PRINCIPLE OF MICROPUMP

A. Structure and Working Principle of Micropump

The proposed micropump is composed of a stack of three wafers bonded together. The micro channel is formed on a glass wafer using a thick photoresist, SU-8, and this channel is filled with electrolyte and a mercury drop is inserted. The movement of the mercury drop pushes or drags the electrolyte, deflecting the membrane which is formed on the second silicon wafer by anisotropic silicon etch. The third wafer, which has passive check valves and holes on the silicon substrate, is stacked on the membrane wafer, forming inlet and outlet chambers. These two chambers are connected through a silicone tube.

Fig. 2 shows the structure of the proposed micropump illustrated with the principle of pump actuation. In step 1, with a positive applied voltage to the electrode, the mercury drop moves toward the outlet chamber and the membrane moves downward, opening the valve in the inlet chamber while closing the valve in the outlet chamber. In this step, the liquid flows into the inlet chamber and comes out from the outlet chamber. In step 2, the polarity of the applied voltage is reversed to make the mercury drop move toward the inlet chamber. The actions in the two chambers are reversed and the liquid in the inlet chamber flows to the outlet chamber through the silicone tube channel. The oscillating mercury motion by alternating applied signals generates a net flow of liquid from the inlet to the outlet.

B. Design of Mercury Path

The gradient in surface tension induced by the externally applied voltage causes a pressure build-up, which initiates the motion of mercury drop. In this moving state of the mercury drop, the mercury is completely surrounded by electrolyte; therefore, the contact angle is considered zero at both ends of the mercury

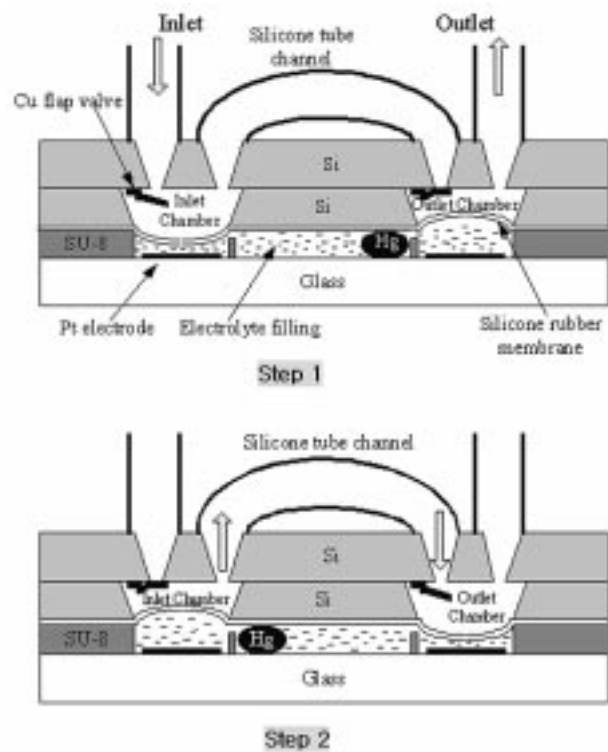


Fig. 2. Schematic view of proposed micropump and the principle of pump actuation.

drop [19]. With this assumption, the pressure build-up by the CEW actuation is given by

$$\Delta P_{CEW} = 2q_0\Delta\phi \left(\frac{1}{D} + \frac{1}{W} \right) \quad (1)$$

where $\Delta\phi$ is the voltage difference between the two ends of the mercury, q_0 is the initial charge per unit area in the electrical double layer in the absence of the applied potential (in most of the aqueous electrolyte, the typical value of q_0 is 0.05 C/m^2), and D and W are the depth and width of the channel, respectively. This equation shows that it is desirable to reduce the channel width and depth for high-pump pressure. However, with reduced channel size, the channel length must be increased for large volume stroke. The volume stroke is ideally equivalent to the channel volume of the mercury path extracting the volume of the mercury drop itself. Because the device size and the resistance of the electrolyte confine the channel length, the optimal channel width, channel depth and channel length must be carefully designed. In this work, the channel length is 4 mm and the cross-sectional area is $500 \mu\text{m} \times 140 \mu\text{m}$; consequently, the volume of spouted electrolyte is $0.21 \mu\text{l}$, which will deflect the membrane up to $30 \mu\text{m}$. Though the channel dimension is not fully optimized yet, the volume stroke of $0.21 \mu\text{l}$ is a sufficient value for micropump operation.

Another important factor that must be considered is the restoring pressure of the deflected membrane. If the restoring pressure of the membrane is larger than the pressure build-up by CEW actuation, the mercury drop will stop before arriving at the mercury stopper placed at the end of the channel. As a result, the volume stroke will be smaller than the channel

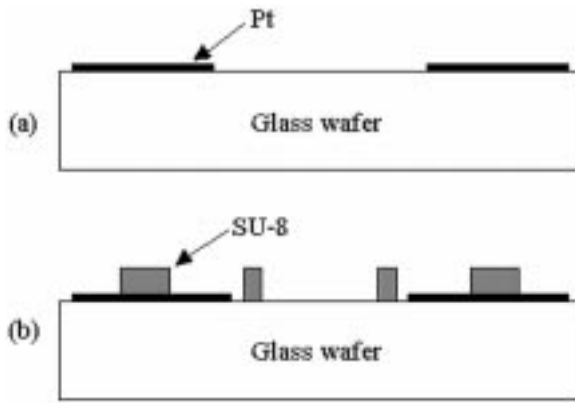


Fig. 3. Fabrication processes for bottom actuator part. (a) Ti/Pt patterning using lift-off. (b) SU-8 spin coating and photo-lithography (thickness = $140 \mu\text{m}$).

volume. The restoring pressure of the deflected membrane can be expressed in the following equation [20]:

$$\Delta P_{\text{membrane}} = 66.138 \frac{Ed}{1-\nu^2} \frac{t^3}{l^4} \quad (2)$$

where E and ν are Young's modulus and Poisson's ratio of the membrane material, respectively, t is membrane thickness, l is the membrane sidewall length, and d is the center deflection. From this equation, when the silicone membrane is deflected about $30 \mu\text{m}$, the restoring pressure is calculated to be about 1.3 Pa , which is much smaller than the pressure generated by CEW actuation. Therefore, in the current design the volume stroke is determined by the channel volume of the mercury path, and it is not affected by the restoring pressure of the membrane.

The mercury drop can travel an infinitely long distance if ideal nonpolarized electrodes are used. However, the platinum electrode is polarized when some amount of current passes through it. Just after the polarization of the electrode, the current decreases to zero and the motion of mercury drop stops. To suppress this phenomenon, we have designed the platinum electrodes at a maximum possible size ($5 \text{ mm} \times 5 \text{ mm}$) that is slightly smaller than the pumping membrane.

IV. FABRICATION

The micropump is composed of three parts—an actuator, membranes, and valves. Each part is individually fabricated and then the components are combined together. This section describes the fabrication processes for each part and the assembly process.

A. Actuator Part

The actuator part is fabricated on a glass wafer to observe the mercury motion as shown in Fig. 3. The platinum electrodes are patterned on a cleaned glass wafer using a lift-off method. A thick photoresist, SU-8 (MicroChem Corp.), is spin-coated and defined at a thickness of $140 \mu\text{m}$, which will form the path for the mercury drop. Fig. 4 shows the fabricated actuator part with a magnified image of the mercury stopper, which prohibits the mercury reaction between the mercury drop and the platinum electrodes.

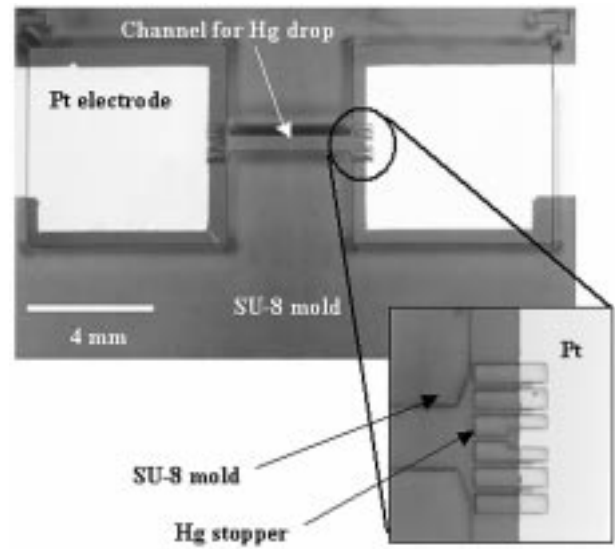


Fig. 4. Photographs of actuator part.

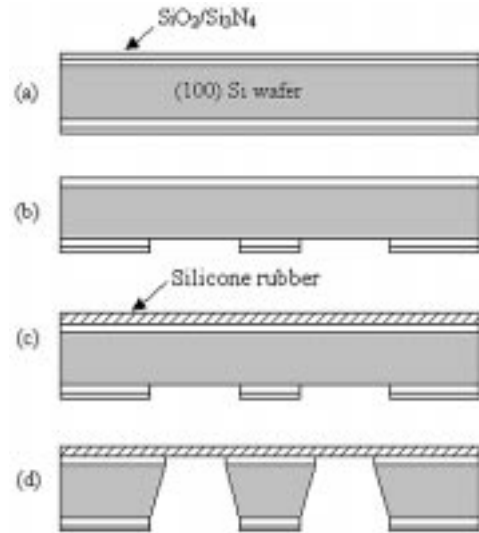


Fig. 5. Fabrication processes for membrane part. (a) Thermal oxidation and deposition of silicon nitride. (b) $\text{SiO}_2/\text{Si}_3\text{N}_4$ patterning on backside using reactive ion etching (RIE). (c) Membrane material coating. (d) Silicon anisotropic etch in KOH solution.

The channel is 4 mm long and has a cross section of $500 \mu\text{m}$ in width and $140 \mu\text{m}$ in depth.

B. Membrane Part

Fig. 5 shows the process sequence for fabricating the membrane part. Thermal oxide is grown on a double-side polished silicon wafer and low pressure chemical vapor deposition (LPCVD) silicon nitride is deposited. Next, the $\text{SiO}_2/\text{Si}_3\text{N}_4$ layer on the backside is patterned and the silicon nitride layer on the front side is removed. The membrane material is silicone rubber (KE1800T, Shin-Etsu Chemical Corporation). The silicone rubber is spin-coated at 5000 rpm for 30 s and cured at $120 \text{ }^\circ\text{C}$ for 1 h and the final thickness of the membrane is about $80 \mu\text{m}$. After deposition of the membrane materials, the silicon wafer is etched in KOH from the backside. Finally, the oxide

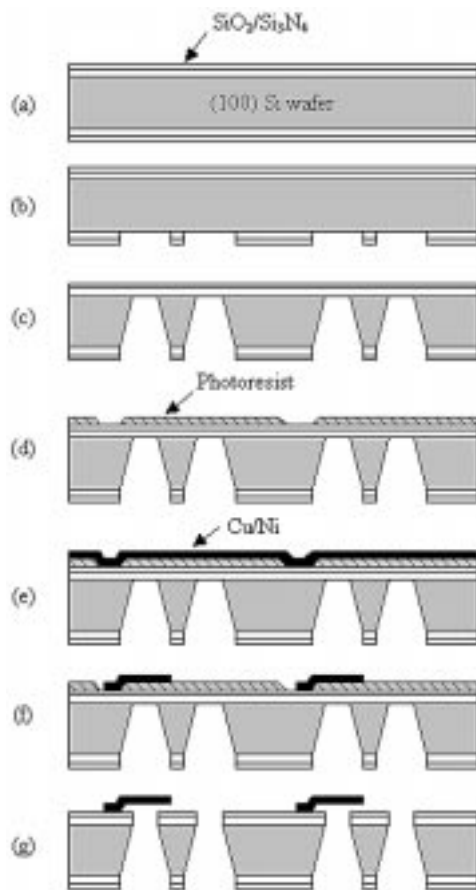


Fig. 6. Fabrication processes for valve part. (a) Thermal oxidation and deposition of silicon nitride. (b) $\text{SiO}_2/\text{Si}_3\text{N}_4$ patterning on backside using RIE. (c) Silicon anisotropic etch in KOH solution. (d) PR patterning (thickness = $1.5 \mu\text{m}$). (e) Ti/Cu evaporation and Cu/Ni electroplating (thickness = $2.5 \mu\text{m}$). (f) Cu/Ni patterning. (g) Removal of sacrificial PR and $\text{SiO}_2/\text{Si}_3\text{N}_4$ layer.

layer under the silicone rubber is etched in a buffered HF solution, defining the membranes whose area is $5.6 \text{ mm} \times 5.6 \text{ mm}$.

C. Valve Part

The fabrication of the valve part starts with a $\text{SiO}_2/\text{Si}_3\text{N}_4$ deposited wafer (Fig. 6). The $\text{SiO}_2/\text{Si}_3\text{N}_4$ layer on the backside is patterned and the bulk silicon is etched in KOH solution. A Ti/Cu seed layer is deposited on a patterned sacrificial photoresist film on the front side and copper is electroplated to a thickness of $2.2 \mu\text{m}$. This electroplated copper has a compressive stress, resulting in valve bending. To compensate for this stress, nickel is electroplated to a thickness of $0.3 \mu\text{m}$ on the top of the plated copper. Next, the electroplated Cu/Ni layer is patterned to form the cantilevers. Finally, the $\text{SiO}_2/\text{Si}_3\text{N}_4$ layer is etched to form the valve holes and the sacrificial photoresist is removed. The cantilever is $660 \mu\text{m}$ long and $310 \mu\text{m}$ wide. The opening size of the valve holes is $180 \mu\text{m} \times 180 \mu\text{m}$.

D. Assembly of Micropump

After the fabrication of the three parts, the electrolyte solution of 0.15-M Na_2SO_4 is filled and a mercury drop is placed in the SU-8 mold and all three parts are assembled and bonded using epoxy bond. The inlet and outlet chambers are connected through a silicone tube which is attached on the wafer using

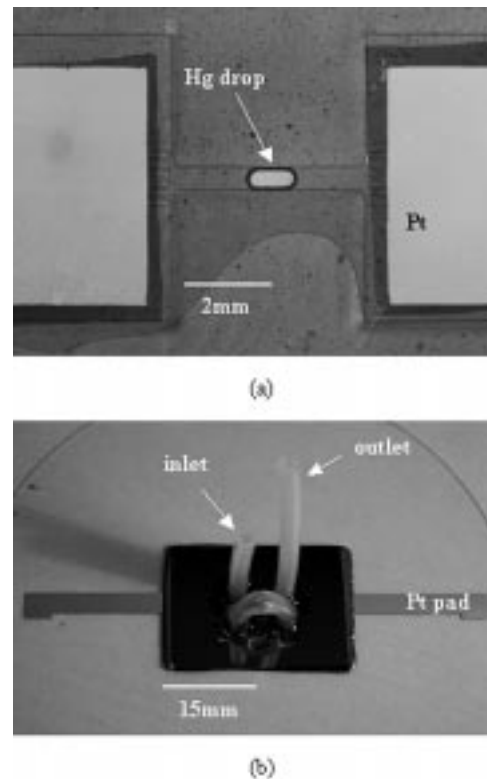


Fig. 7. Photographs of assembled micropump. (a) Mercury-placed actuator part. (b) Assembled micropump.

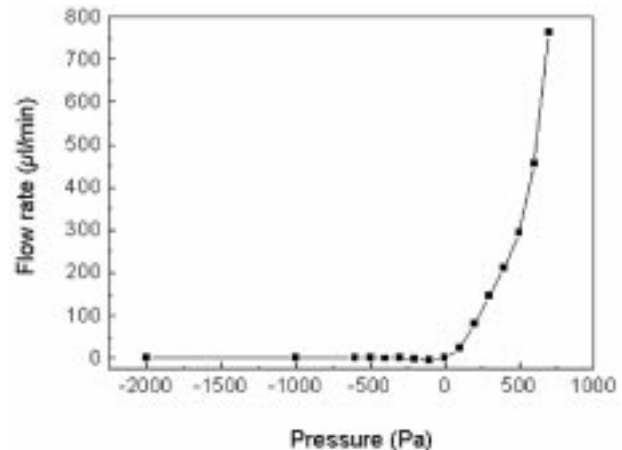


Fig. 8. Measured valve characteristics.

epoxy. Fig. 7 shows a photograph of the fabricated mercury-placed actuator part and the assembled micropump.

V. EXPERIMENTAL RESULTS AND DISCUSSION

A. Valve Characteristics

The relationship between applied pressure and flow rate of the fabricated check valves is illustrated in Fig. 8. The static leakage of the valve in reverse pressure is observed to be less than about $4 \mu\text{l}/\text{min}$ at lower pressures. However, the valve closes completely when the reverse pressure is over 300 Pa and the leakage is negligible in the range of the operating pressure of the micropump, which is about 700 Pa. At a pressure of

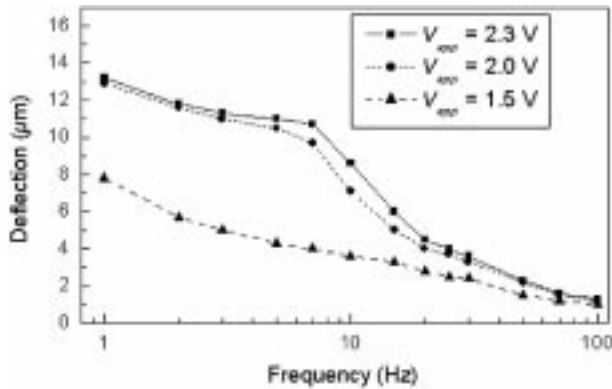


Fig. 9. Measured deflection of silicone rubber membrane (thickness = $80 \mu\text{m}$).

700 Pa in the forward direction, the flow rate is measured to be about $800 \mu\text{l}/\text{min}$, which is sufficient for the operation of the micropump.

B. Membrane Deflection

The center deflection of the pumping membrane has been measured using a laser displacement meter (LC-2420, Keyence Corp.). Fig. 9 shows the measurement data for the $5.6 \text{ mm} \times 5.6 \text{ mm} \times 80 \mu\text{m}$ silicone rubber membrane. The maximum deflection for the silicone rubber has been measured as $13 \mu\text{m}$.

As was explained in the previous section, the silicone rubber has a very low Young's modulus (about 0.98 MPa). Therefore, very little pressure is required to deflect the membrane. The center deflection of the membrane is dominated by the channel volume of the mercury path, not by the pressure of the CEW actuation. If there is no leakage through the gap between the mercury drop and sidewall, the volume stroke is identical to the volume of the pushed electrolyte by the mercury drop. The shape of the deflected membrane has been simulated using finite element analysis (ANSYS) and fitted by sinusoidal functions. By using this equation, we can derive the center deflection of the membrane from the volume stroke. In this work, the pushed electrolyte is assumed to be about $0.21 \mu\text{l}$ and the center deflection of the membrane is simulated at about $30 \mu\text{m}$. This calculated value is approximately double the experimental number of $13 \mu\text{m}$. The difference between these two values seems to arise from the leakage of the electrolyte through the corner gap between the mercury drop and the sidewall. More study is required to identify the discrepancy.

In the frequency range tested, the center deflection decreases as the operation frequency increases, as shown in Fig. 9. At lower frequencies, the mercury drop moves along the nearly full length of channel path, resulting in little variation of the membrane deflection with respect to frequency. However, at higher frequencies, the mercury drop starts to travel less than the channel length, resulting in a reduction of electrolyte displacement and membrane deflection. We speculate that secondary effects become nonnegligible when the frequency is high and travel distance is short, such as acceleration/deceleration period and imperfection in fabrication (e.g., leakage, trapped gas).

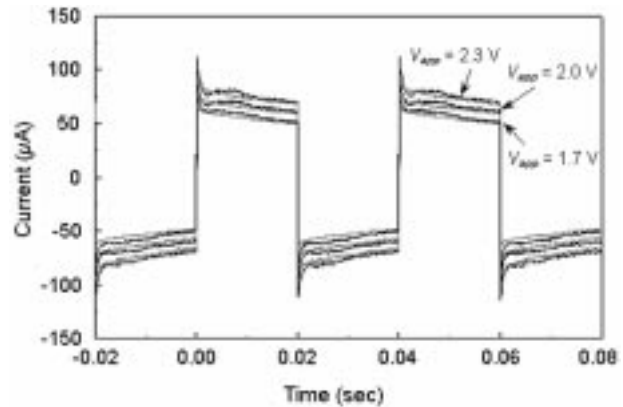


Fig. 10. Driving current for various operation voltages at 25 Hz (Black line for the channel with Hg drop and gray line for channel without Hg drop).

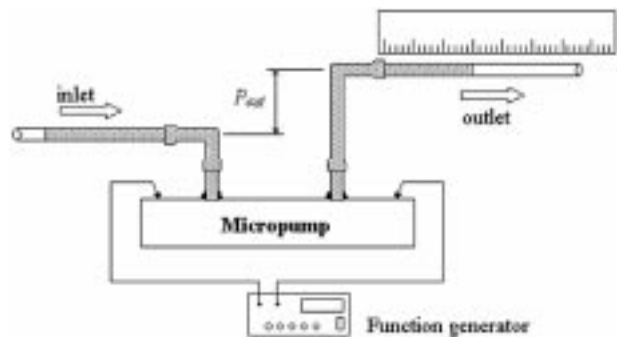


Fig. 11. Measurement set-up.

C. Power Consumption

The driving current is measured using a low noise current amplifier (SR570, Stanford Research Systems Corp.), which is connected in series with the micropump electrodes. Fig. 10 shows the measured waveform of the driving current for three operation voltages. The black lines are the driving currents for the channels with a mercury drop and the gray lines indicate the channels without a mercury drop. Each applied voltage is a rectangular waveform of a frequency of 25 Hz. With the operation voltages of 2.3 V, 2.0 V, and 1.7 V, the average power consumption is about $170 \mu\text{W}$, $120 \mu\text{W}$, and $90 \mu\text{W}$, respectively. This figure also shows that the average driving current is slightly smaller in the channels without mercury drops than in the ones with mercury drops.

D. Flow Rate, Pump Pressure, and Performance Comparison

The measurement setup for the micropump is depicted in Fig. 11. Rectangular waveform voltages with various amplitudes and frequencies have been applied to the pads. The flow rate is calculated by measuring the moving distance of the liquid surface in a glass capillary for a given time. The pressure at the outlet P_{out} is obtained by locating the inlet and outlet ports at different heights. Prior to the experiment, liquid is supplied into the device, so that the pump chamber is filled and a meniscus is formed in the capillary. In this experiment, the pumping liquid is deionized water.

Fig. 12 shows the measured flow rates of the micropump using silicone rubber membranes when the square wave volt-

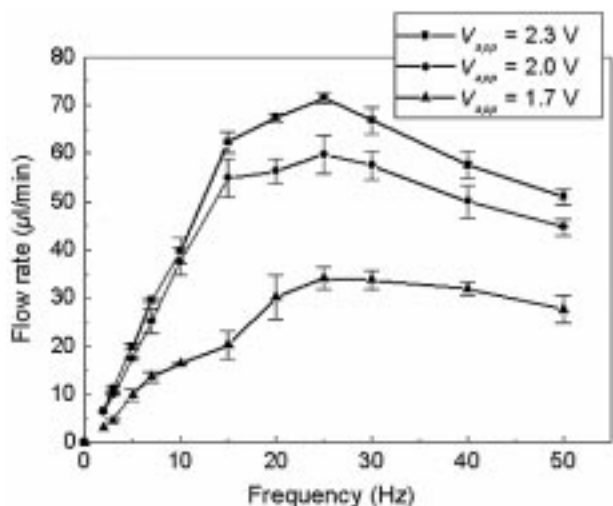


Fig. 12. Flow rates as a function of the actuation frequency.

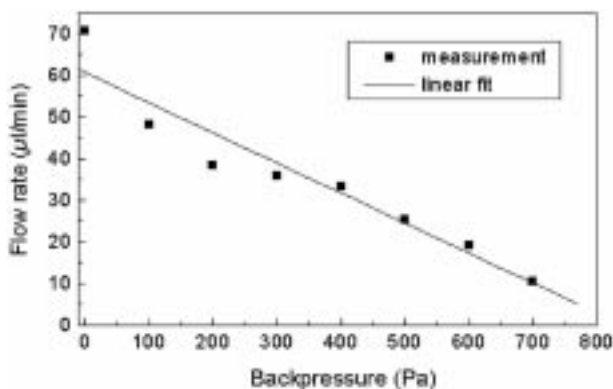


Fig. 13. Flow rate versus backpressure characteristics for actuation voltage of 2.3 V at 25 Hz.

ages are applied without backpressure. All measurements have been performed three times. The maximum flow rate is measured as 70 $\mu\text{l}/\text{min}$ at a frequency of 25 Hz with an applied voltage of 2.3 V. The flow rate is proportional to the product of the operation frequency and membrane deflection. In the low frequency range, the flow rate increases according to the frequency increment. However, the flow rate decreases in the upper frequency range, above 25 Hz, as the membrane deflection abruptly decreases as was explained in the previous section.

The linear dependence between the flow rate and the applied backpressure on the outlet is shown in Fig. 13. A maximum pump pressure of about 800 Pa has been measured at the applied voltage of 2.3 V with the operation frequency of 25 Hz. If we neglect the pressure required to deflect the membranes and the flap valves, the maximum pump pressure is determined by the pressure build-up by CEW actuation that is directly proportional to the voltage difference between the two ends of the mercury ($\Delta\phi$), as was expressed in (1). Though it is quite difficult to ascertain an accurate value for this voltage difference ($\Delta\phi$), we calculated the rough value by multiplying the driving current by the impedance of the mercury drop region, which was extracted from experimental data.

Fig. 14 shows the electrical equivalent model for a CEW system where Z_i is the equivalent impedance of the metal–elec-

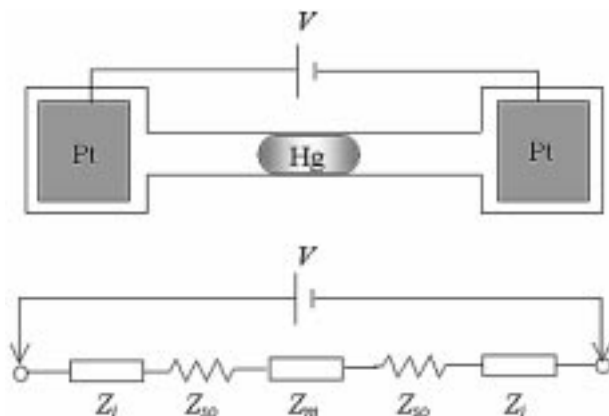


Fig. 14. Electrical equivalent model for a CEW system.

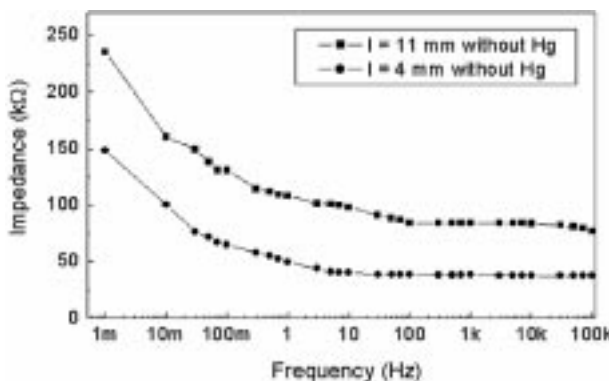


Fig. 15. The impedance between two electrodes of the CEW system without Hg drop.

trolyte interface, Z_{so} is the solution impedance, and Z_m is the impedance of the mercury drop region [17]. Each of these impedances includes some capacitors and resistors including double layer capacitance. However, for convenience of obtaining the voltage difference between the two ends of the mercury, the metal–electrolyte interface has been modeled by a simple impedance equivalent circuit. The magnitude of the voltage applied on the mercury drop can be calculated by multiplying the driving current to the impedance of the mercury drop region (Z_m). The impedance between the two electrodes of the CEW system without a mercury drop has been calculated by measuring the currents for applied sinusoidal voltages of various frequencies, as shown in Fig. 15. The rectangular and circular symbols represent the experimental results using 11-mm and 4 mm-long channels, respectively, filled with 0.15-M Na_2SO_4 solution. The impedance difference for the two different channel lengths is constant for the entire range of frequencies. This shows that the solution impedance (Z_{so}) is a pure resistive component and can be calculated to be approximately 7.14 $\text{k}\Omega/\text{mm}$.

It should be noted again from Fig. 10 that the driving current is very similar for the two cases with or without a mercury drop. Actually, the average driving current for this 4-mm-long channel without a mercury drop is about 75 μA for the operation voltage of 2.3 V and the voltage applied on the electrolyte in the channel is about 0.54 V/mm. Because the voltages applied on metal–electrolyte interface and electrolyte are the same for

TABLE I
PERFORMANCE COMPARISON OF MICROPUMPS

Actuator Type	Maximum flow rate ($\mu\text{l}/\text{min}$)	Operation voltage (V)	Power consumption (mW)	Maximum pump pressure (kPa)	Reference
Piezoelectric	1500	180	-	98	[2]
	40	180	-	15	[3]
Electrostatic	550	280	1	31	[5]
Thermopneumatic	6.3	-	293	32	[9]*
	34	6	2800	4	[9]
Electromagnetic	20	3	908	-	[10]
Electrostatic	45	18	-	-	[11]
MEMS	50	-	638	-	[12]
CEW	70	2.3	8.17	9.8	Our work

* Peristaltic type without passive check valves

these two cases, the actual voltage drop across the two ends of the mercury drop (which is about 1 mm) will be very close to the one applied on the electrolyte of the same length. Therefore, the pump pressure can be estimated from the pressure created by CEW as given in (1), which is about 500 Pa from the given numbers: $\Delta\phi$ of 0.54 V, D of 140 μm , and W of 500 μm . This estimated value was calculated using average driving current. In fact, the instantaneous pressure and the consequent pump pressure should be larger than this calculated value. When the device is vertically mounted, the gravitational force may influence the motion of the mercury drop. For the device tested in this paper, the pressure on mercury drop by gravity is calculated to be about 130 Pa, a nonnegligible fraction of the CEW actuation pressure. However, as the influence of the gravity is proportional and the actuation pressure is inversely proportional to channel size, the gravity effect can be ignored for the next generation devices with more shallow channels.

In Table I, the performance of the proposed micropump is compared with those of previous micropumps operated by various actuation mechanisms. Though this table does not show the reported data with fair normalization in detail, we observe that with extremely low power consumption and low-operation voltage, the proposed micropump achieves comparable performance.

E. Reliability

With the operation voltage of 2.3 V and 25 Hz, the fabricated micropump operated with little decrease in flow rate for 20 h, which is equivalent to 2×10^6 pumping cycles. After that period, the motion of the mercury drop slowed down and finally stopped, resulting in failure of pump operation. The main source for the failure is the contamination of the mercury drop [17] and this problem can be resolved by using another material for the mercury channel. However, we have not observed any electrolysis below the applied voltage of 2.5 V. In the case of higher applied voltages above 3 V, we have observed the electrolysis of the electrolyte on the Pt electrode or breakage of the mercury drop caused by the bidirectionally induced gradient of surface tension [19].

VI. CONCLUSION

This paper has described the development of a surface-tension driven micropump utilizing CEW phenomenon. The CEW

actuation uses local variation of surface tension for generating motion. All parts of the micropump, including check valves, silicone rubber membranes and a CEW actuator, have been fabricated using MEMS-based technologies, and the actuation of the micropump has been successfully demonstrated.

The center deflection of pumping membrane has been measured for various operation voltages and frequencies, showing a maximum deflection of about 13 μm . The fabricated check valve has shown good operation for both directions of applied pressure. The operation voltage of the fabricated micropump was below 2.3 V and the power consumption was lower than 170 μW . The maximum flow rate was measured to be about 70 $\mu\text{l}/\text{min}$ at a frequency of 25 Hz with an applied voltage of 2.3 V, and a maximum pump pressure of about 800 Pa was obtained.

The proposed micropump has achieved comparable performance to previous micropumps operated by various actuation mechanisms with extremely low power consumption and low voltage operation and can be used in application fields such as handheld micro lab-on-a-chips and portable biomedical devices where large pump pressure is not required. Further improvements of device fabrication are under development for more reproducible and reliable fabrication—including replacement of the silicone tube channel with a patterned glass substrate or polydimethylsiloxane (PDMS), electrodeposition of the mercury drop and local sealing of the microfluidic CEW actuators using permanent bonding methods such as anodic bonding.

ACKNOWLEDGMENT

The authors would like to thank G.-H. Kim and Y.-S. Jeon for their initial help on SU-8 processes and Prof. J. Kwak, D.-H. Lee and K.-H. Chung for their helpful discussions.

REFERENCES

- [1] S. Shoji, "Fluids for sensor systems," *Top. Current Chem.*, vol. 194, pp. 163–188, 1998.
- [2] D. Maillefer, H. Van Lintel, G. Rey-Mermet, and R. Hirschi, "A high-performance silicon micropump for an implantable drug delivery system," in *Proc. 12th IEEE MEMS '99*, Orlando, FL, pp. 541–546.
- [3] R. Linnemann, P. Woias, C.-D. Senft, and J. A. Ditterich, "A self-priming and bubble-tolerant piezoelectric silicon micropump for liquid and gases," in *Proc. 11th IEEE MEMS '98*, Heidelberg, Germany, pp. 532–537.
- [4] S. Shoji, S. Nakagawa, and M. Esashi, "Micropump and sample-injector for integrated chemical analyzing systems," *Sens. Actuators A, Phys.*, vol. 21–23, pp. 189–192, 1990.
- [5] R. Zengerle, S. Kluge, M. Richter, and A. Richter, "A bidirectional silicon micropump," in *Proc. IEEE MEMS '95*, Amsterdam, Netherlands, pp. 19–24.
- [6] J. W. Judy, T. Tamagawa, and D. L. Polla, "Surface-machined microchannel membrane pump," in *Proc. IEEE MEMS '91*, Nara, Japan, pp. 182–186.
- [7] O. C. Jeong and S. S. Yang, "Fabrication and test of a thermopneumatic micropump with a corrugated p^+ diaphragm," *Sens. Actuators A, Phys.*, vol. 83, pp. 249–255, 2000.
- [8] C. Grosjean and Y.-C. Tai, "A thermopneumatic peristaltic micropump," in *Proc. 10th Int. Conference on Solid-State Sensors and Actuators*, Sendai, Japan, 1999, pp. 1776–1779.
- [9] F. C. M. Van De Pol, H. T. G. Van Lintel, M. Elwenspoek, and J. H. J. Fluitman, "A thermopneumatic micropump based on micro-engineering techniques," *Sens. Actuators A, Phys.*, vol. 21–23, pp. 198–202, 1990.
- [10] W. Zhang and C. H. Ahn, "A bidirectional magnetic micropump on a silicon wafer," in *Proc. IEEE Solid-State Sensor and Actuator Workshop*, Hilton Head, SC, 1996, pp. 94–97.

- [11] Y. Yang, Z. Zhou, X. Ye, and X. Jiang, "A bimetallic thermally actuated micropump," *Microelectromech. Syst. (MEMS)*, ASME, vol. DSC-59, pp. 351–354, 1996.
- [12] W. L. Benard, H. Kahn, A. H. Heuer, and M. A. Huff, "Thin-film shape-memory alloy actuated micropumps," *J. Microelectromech. Syst.*, vol. 7, pp. 245–251, 1998.
- [13] G. Beni, S. Hackwood, and J. L. Jackel, "Continuous electrowetting effect," *Appl. Phys. Lett.*, vol. 40, no. 10, pp. 912–914, May 1982.
- [14] J. L. Jackel, S. Hackwood, J. J. Veslka, and G. Beni, "Electrowetting switch for multimode optical fibers," *Appl. Opt.*, vol. 22, no. 11, pp. 1765–1770, Jun. 1983.
- [15] H. Matsumoto and J. E. Colgate, "Preliminary investigation of micropumping based on electrical control of interfacial tension," in *Proc. IEEE MEMS '90*, Napa Valley, CA, Feb. 1990, pp. 105–110.
- [16] J. Ni, C.-J. Zhong, S. J. Coldiron, and M. D. Porter, "Electrochemically actuated mercury pump for fluid flow and delivery," *Anal. Chem.*, vol. 73, pp. 103–110, 2001.
- [17] J. Lee and C. J. Kim, "Surface tension driven microactuation based on continuous electrowetting (CEW)," *J. Microelectromech. Syst.*, vol. 198, pp. 171–180, 2000.
- [18] T. D. Truong, "Selective deposition of micro scale liquid gallium alloy droplets," M.S. thesis, University of California, Los Angeles, CA, 2000.
- [19] J. Lee, "Microactuation by continuous electrowetting and electrowetting: Theory, fabrication, and demonstration," Ph.D. dissertation, University of California, Los Angeles, CA, 2000.
- [20] S. Timoshenko and S. Woinowsky-Krieger, *Theory of Plates and Shells*, 2nd ed, New York: McGraw-Hill, 1959, ch. 6.



Kwang-Seok Yun received the B.S. degree in electrical engineering from Kyungpook National University, Daegu, Korea, in 1996 and the M.S. degree in electrical engineering from Korea Advanced Institute of Science and Technology (KAIST), Daejeon, Korea, in 1999. He is currently a Ph.D. candidate in electrical engineering and computer science, KAIST.

His current research interests include bio-MEMS, microfluidics, and miniaturized analytical systems.



Il-Joo Cho received the B.S. and M.S. degrees in electrical engineering from Korea Advanced Institute of Science and Technology (KAIST), Daejeon, Korea, in 1998 and 2000, respectively. Since then, he has been working as a Ph.D. candidate student at the same institute.

His current research interests are in the micromirrors for optical communication and electromagnetic actuators.

Jong-Uk Bu received the Ph.D. degree in metallurgical engineering from Korea University in 1992.

Since 1984, he has been with LG Electronics Institute of Technology, Seoul, Korea, where he has worked on the area of silicon micromachining and micro-sensors. From 1995 to 1996, he has been with the Center for Integrated Sensors and Circuits, Department of Electrical Engineering and Computer Science, University of Michigan, Ann Arbor, as a Visiting Scholar. Currently, he is in charge of MEMS research and business in LG Electronics Institute of Technology as a group leader of Microsystem group and MEMS Product group. His research interests include development of microfabrication and micromachining technologies for microsystem; micro sensors, optical communication components, RF MEMS, and MEMS embedded high density data storage systems. He has published and presented more than 100 MEMS-related technical papers and 90 patents.



Chang-Jin "CJ" Kim received the B.S. degree from Seoul National University and the M.S. degree from Iowa State University, Ames, along with the Graduate Research Excellence Award. He received the Ph.D. degree in mechanical engineering from the University of California at Berkeley in 1991.

Since joining the faculty at the University of California, Los Angeles (UCLA) in 1993, he has developed several MEMS courses and established a MEMS Ph.D. major field in Mechanical and Aerospace Engineering Department. His research

is in MEMS and nanotechnology, including design and fabrication of micro/nanostructures, actuators, and systems, with a recent focus on the use of surface tension.

Prof. Kim served as Chairman of the Micromechanical Systems Panel of the ASME DSC Division and coorganized the MEMS Symposia between 1994 and 1996 for the ASME International Mechanical Engineering Congress and Exposition. He also organized the 1996 ASME Satellite Broadcast Program on MEMS and the 6th IEEE International Conference on Emerging Technologies and Factory Automation. He served in various Technical Program Committees, including the IEEE MEMS Conference, Transducers, and the SPIE Symposium on Micromachining and Microfabrication. Currently he is serving in the U.S. Army Science Board as Consultant, in the Executive Committee of ASME MEMS Subdivision, and as a Subject Editor for the IEEE/ASME Journal of MEMS. He is the recipient of the 1995 TRW Outstanding Young Teacher Award and the 1997 NSF CAREER Award.



Euisik Yoon received the B.S. and M.S. degrees in electronics engineering from Seoul National University, Korea, in 1982 and 1984, respectively, and Ph.D. degree in electrical engineering from the University of Michigan, Ann Arbor, in 1990.

From 1990 to 1994, he was with the Fairchild Research Center of the National Semiconductor Corporation, Santa Clara, CA, where he was engaged in researches on deep submicron CMOS integration and advanced gate dielectrics. From 1994 to 1996, he was a Member of Technical Staff at Silicon Graphics, Inc.,

Mountain View, CA, working on the design of the MIPS microprocessor R4300I and the RCP3-D graphic coprocessor. In 1996, he joined the Department of Electrical Engineering at Korea Advanced Institute of Science and Technology (KAIST), Daejeon, Korea, where he is now an Associate Professor. His present research interests are in MEMS, integrated microsystems, and VLSI circuit design. He served in various Technical Program Committees including Microprocesses and Nanotechnology Conference and IEEE Asia-Pacific Conference on ASIC's. Currently, he is serving in IEEE ISSCC Imager/MEMS/Display subcommittee.